Preparation of Bi-based heterostructures through calcination with potential photocatalytic application

Eduardo H. Dias[a,b], Gelson T. S. T. da Silva[a,1], Osmando F. Lopes[c], and Caue Ribeiro[a]

[a] Nanotechnology National Laboratory for Agriculture (LNNA), Embrapa Instrumentation, 13561206, São Carlos - SP, Brazil.
[b] São Carlos Institute of Chemistry, University of São Paulo, 13560970, São Carlos - SP, Brazil.
[c] Laboratory of Photochemistry and Materials Science, Institute of Chemistry, Federal University of Uberlândia, 38400902, Uberlândia - MG, Brazil.

*e-mail: gelsonttavares@gmail.com

_____

Abstract. In this study, we reported a facile method to obtain Bi-based heterostructures by a calcination process. The temperature of the treatment changed the crystalline phase of the sample, so it was possible to produce $(BiO)_2CO_3$, α-Bi_2O_3, and β-Bi_2O_3 pure phases and $(BiO)_2CO_3/\alpha$-Bi_2O_3 and α-Bi_2O_3/β-Bi_2O_3 heterostructures. Moreover, the heating also influenced morphology and optical and photocatalytic properties of the materials. The bandgap of the synthesized samples above 350ºC demonstrates the possibility of using these materials in catalytic processes driven by visible radiation. The photocatalytic tests under UV light showed that the $(BiO)_2CO_3$ sample has a higher activity for degradation of the methylene blue (MB) than the Bi_2O_3 discoloring 91% and 38%, respectively. On the other hand, the photocatalysis under visible light showed that samples treated above 300°C have good performance under visible radiation, inducing up to 56% degradation of methylene blue. These results demonstrate that increasing temperature impairs the photocatalytic efficiency of Bi-based samples under UV radiation, however, improves the activity for tests conducted by visible radiation that may be attributed to the bandgap reduction and the electron/hole pair lifetime increasing.

Keywords: Heterogeneous Photocatalysis, Water Treatment, $(BiO)_2CO_3$, Heterojunctions

_____

1. Introduction

In recent years, heterogeneous photocatalysis has become a promising alternative in both wastewater treatment and air pollution mitigation, due to its ability to use light source as a trigger to conduct these processes, especially sunlight.[1,2] In the photocatalysis process, after activated, a semiconductor generates reducing and oxidizing charges carriers (electron/holes) in its valence and conduction band and these species can lead to degradation

of organic molecules by direct or indirect oxidation, through the generation of radicals ($^\bullet$OH, $^\bullet$O$_2$).[3,4]

Typically, metal oxides such as TiO_2 and ZnO are the most popular materials used as photocatalysts.[5–8] These materials are activated only under UV radiation, so they have low efficiency driven by solar radiation, making large-scale applications inviable.[9] Thus, there has been a growing interest in developing functional materials capable of absorbing a larger part of the solar spectrum, as active catalysts under visible radiation, as this represents 43% of sunlight, against only 5% for UV radiation.[10]

Bismuth compounds are interesting and can be promising candidates even in different forms, i.e., BiOX has been used in carbon dioxide photoreduction,[11] Bi_2S_3 has been applied to boost the hydrogen photogeneration,[12] Bi_2O_3 has been used as gas sensors, solid oxide fuel cells, optical coatings, and ceramic glass manufacturing,[13] and $BiVO_4$ has been studied for oxygen evolution and organic pollutant degradation.[14]

The $Bi_2O_2CO_3$ is a good catalyst to degrade pollutants, but its band gap is 3.5 eV wich means that this semiconductor can be activated only under UV irradiation.[15] However, some Bi-based semiconductors, especially bismuth oxide (Bi_2O_3), has high solar spectrum absorption (~2.5 eV), but these materials have high recombination of photo-generated charge carriers and this inconvenience causes limitations in its catalytic performance.[16] Thus, the construction of a heterojunction between two semiconductors can minimize this effect, increasing the charge carrier lifetime, due to spatial separation in the photogenerated electron/hole pairs.[17]

The heterostructures formation improving the performance of the catalysts compared to the isolated phase.[18] Nevertheless, the formation of suitable heterostructures could require successive steps, significantly altering the efficiency of the process.[19] Some examples of heterojunction formation are the reactions where preformed materials are coupled to semiconductors due to changes in pH,[20] pressure,[21] and temperature,[22] making the process unreproductive.[23]

Therefore, this work aims to show an easy way to synthesize Bi-based heterostructures through a facile method and use the produced compounds for the photooxidation of organic pollutants. Besides characterizing structurally, electrically, and morphologically, the study aims to understand the effect of calcination treatment and the correlation with the photocatalytic capacity of the prepared samples.

2. Material and Methods

1.1. Synthesis

The Bi-based heterostructures were synthesized by a calcination method using bismuth subcarbonate (($BiO)_2CO_3$) (Sigma Aldrich) as a precursor. Briefly, 0.5 g of $(BiO)_2CO_3$ powder was placed in a 40 mL alumina crucible and positioned at the center of a muffle furnace (EDG 1800) and heated at different temperatures (300, 350, 370, and 400ºC) for 2 h, using a heating rate of 5°C min^{-1}. After the heating process, the furnace was cooled to room temperature, thus completing the synthesis. The powder was then collected and finely grounded in an agate mortar.

1.2. Characterization

A Shimadzu XRD 6000 diffractometer was used to determine the crystal structure of the catalysts, with CuKα radiation and scanned for 2θ values from 10 to 60°. The morphology and particle size of the synthesized samples were analyzed by scanning electron microscopy (SEM) JEOL JEM 2010), and the optical properties were recorded using a UV–vis spectrophotometer in the range 275–800 nm (Shimadzu UV-2600) equipped with an integrating sphere (ISR-2600 Plus). From UV–vis diffuse reflectance spectra data were estimated the bandgap energies by Tauc equation. Raman spectra were recorded on an FT-Raman spectrometer (Bruker RAM II with a Ge detector) using an Nd:YAG laser with the excitation wavelength of 1064 nm.

1.3. Catalytic performance

The photooxidation performance of the as-synthesized samples was evaluated, monitoring the methylene blue (MB) discoloration under UV and visible irradiation. In a typical procedure, 10 mg of the photocatalyst was placed in 20 mL of MB dye solution (5 mg L^{-1}). Before starting the photocatalytic experiments, the suspensions were stirring overnight in dark conditions to reach the adsorption/desorption equilibrium. All experiments were performed at 18°C on a photoreactor equipped with six germicidal lamps (Osram, 15 W, $\lambda_{maximum}$= 254 nm) and fluorescent lamps (Phillips, 15 W, $\lambda_{maximum}$= 440 nm) for the evaluation of photoactivity under UV and visible radiation, respectively. During the catalytic tests, the maximum absorbance of the MB (668 nm) was monitored at regular intervals using a Shimadzu UV-1601 PC spectrophotometer.

3. Results and discussion

1.4. Characterization

The crystalline phase changes and the heterostructure formation due to calcination treatment of $Bi_2O_2CO_3$ were evaluated by XRD analysis (Figure 1). It was observed that the XRD pattern of the precursor could be indexed with $(BiO)_2CO_3$ (JCPDS: 41-1448) without any impurities. It can be observed that $(BiO)_2CO_3$ sample was stable up to 300°C. On the other hand, when the sample was treated at 350ºC it was observed a mixed-phase between $(BiO)_2CO_3$ and β-Bi_2O_3 in the crystalline tetragonal phase (JCPDS: 27-0050) because the $(BiO)_2CO_3$ was partially decomposed in β-Bi_2O_3 according to the following reaction: $(BiO)_2CO_3 \rightarrow Bi_2O_3 + CO_2$. The $(BiO)_2CO_3$ sample was completely decomposed when calcinated at 370ºC, it was observed the formation of β-Bi_2O_3. The increase in the calcination temperature to 380ºC resulted in a mixed-phase between β-Bi_2O_3 and α-Bi_2O_3 (JCPDS: 41-1449). Finally, when $(BiO)_2CO_3$ was annealed at 400ºC, it was obtained the α-Bi_2O_3 pure. Therefore, the proposed method was efficient to obtain the pure phases ($(BiO)_2CO_3$, β-Bi_2O_3, and α-Bi_2O_3) as well as the mixed phases ($(Bi_2O)_2CO_3$/β-Bi_2O_3 and β-Bi_2O_3/α-Bi_2O_3). Thermogravimetric analysis (TGA) of $Bi_2O_2CO_3$ sample were performed to evaluate the thermal decomposition (i.e., the formation of Bi_2O_3 by the loss of carbonate group). As shown in Figure 2, the $Bi_2O_2CO_3$ sample lost 9.0% of its initial mass, due to the total decomposition of the carbonate group.[24] The analysis of the derivative thermogravimetry (DTG) curves showed that the decomposition temperature of $Bi_2O_2CO_3$ occurs at 356°C in close agreement with the XRD results.
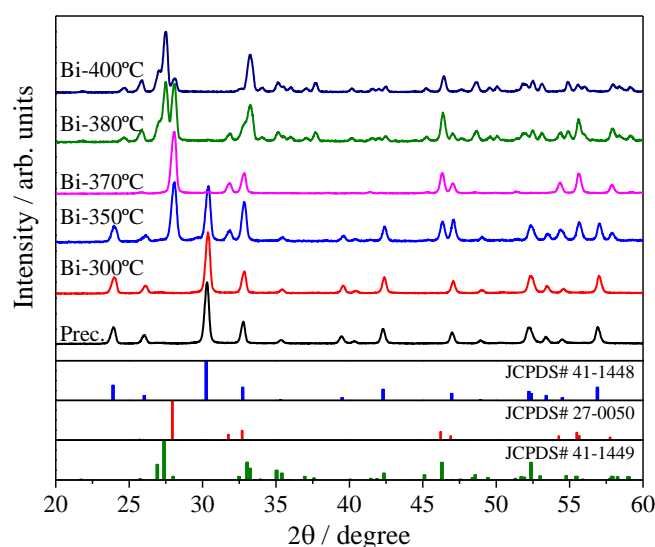
Figure 1 – X-ray diffraction patterns of the $(BiO)_2CO_3$ samples annealed in different temperatures. Blue (precursor), red lines (beta phase), and green lines (alpha phase).
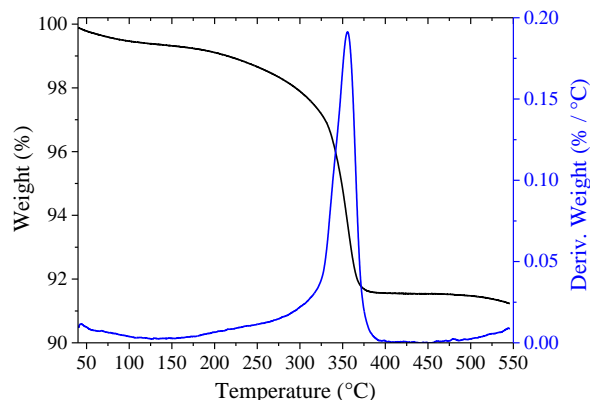
Figure 2 – Thermogravimetric analysis (TGA) and derivative (DTG) for $Bi_2O_2CO_3$ sample.

The effect of $(BiO)_2CO_3$ calcination on its local structure was evaluated by Raman scattering spectra (Figure 3). The precursor sample showed a typical Raman spectrum of $(BiO)_2CO_3$, with characteristic bands at 1068, 367, 166, and 80 cm^{-1}. The band at 1068 cm^{-1} was assigned to symmetric stretching of CO_3^{-2}, while the three bands below 400 cm^{-1} were related to vibrational modes of Bi=O bond lattice.[24] It was not verified any modification in the Raman spectrum of $(BiO)_2CO_3$ sample annealed at 300ºC. However, the temperature increase to 350ºC decreases the peaks related to $(BiO)_2CO_3$ and arises 5 typical peaks (70, 91, 127, 232, 315, and 467 cm^{-1}) from β-Bi_2O_3. The sample annealed at 370 ºC showed several peaks that could be related to both Bi_2O_3 phases (β and α) different from XRD results that showed β-Bi_2O_3 pure. The α-Bi_2O_3 sample are identified by the following peaks: 70, 95, 122, 141, 153, 186, 213, 315, 413, 450, and 542 cm^{-1}.[25] The Raman scattering peaks observed in the region below 120 cm^{-1} are mainly assigned to shifts in the Bi atoms. The peaks in the range from 120 to 150 cm^{-1} are attributed to shifts in the Bi and O atoms, and those above 150 cm^{-1} were assigned to displacements of the O atoms. This difference is related to the sensitivity of both techniques, besides the peaks related to the α-Bi_2O_3 phase overlapping the peaks of the β-Bi_2O_3 phase.
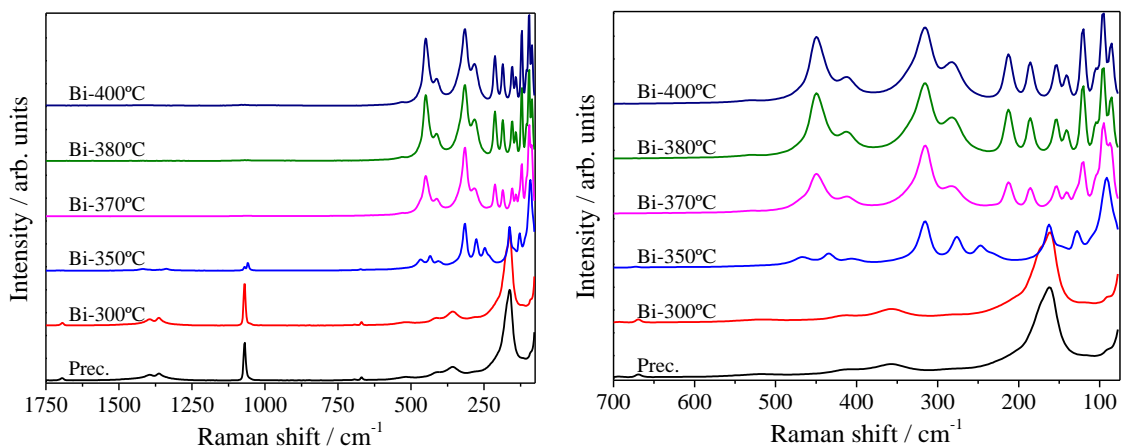
Figure 3 – The Raman Spectra of $(BiO)_2CO_3$ pristine and calcined at different temperatures (a), with a cut-off in the region 700 - 75 cm^{-1} (b).

The scanning electron microscopy (SEM) was used to evaluate the morphologies of the samples (Figure 4). The $(BiO)_2CO_3$ sample exhibited micrometric sheets with the nanometric thickness that is a typical morphology of this phase (Figure 4a). The sample's morphology was not significantly changed up to 300ºC, in agreement with observed by XRD and Raman spectra. However, the increase of the calcination temperature to 350ºC causes a change in morphology making the micrometric sheets in plate denser (Figure 4b). The sample treated at 370ºC also exhibited the plate-like morphology (Figure 4c). However, the sample treated at 380 and 400ºC exhibited micrometric particles with different morphologies.
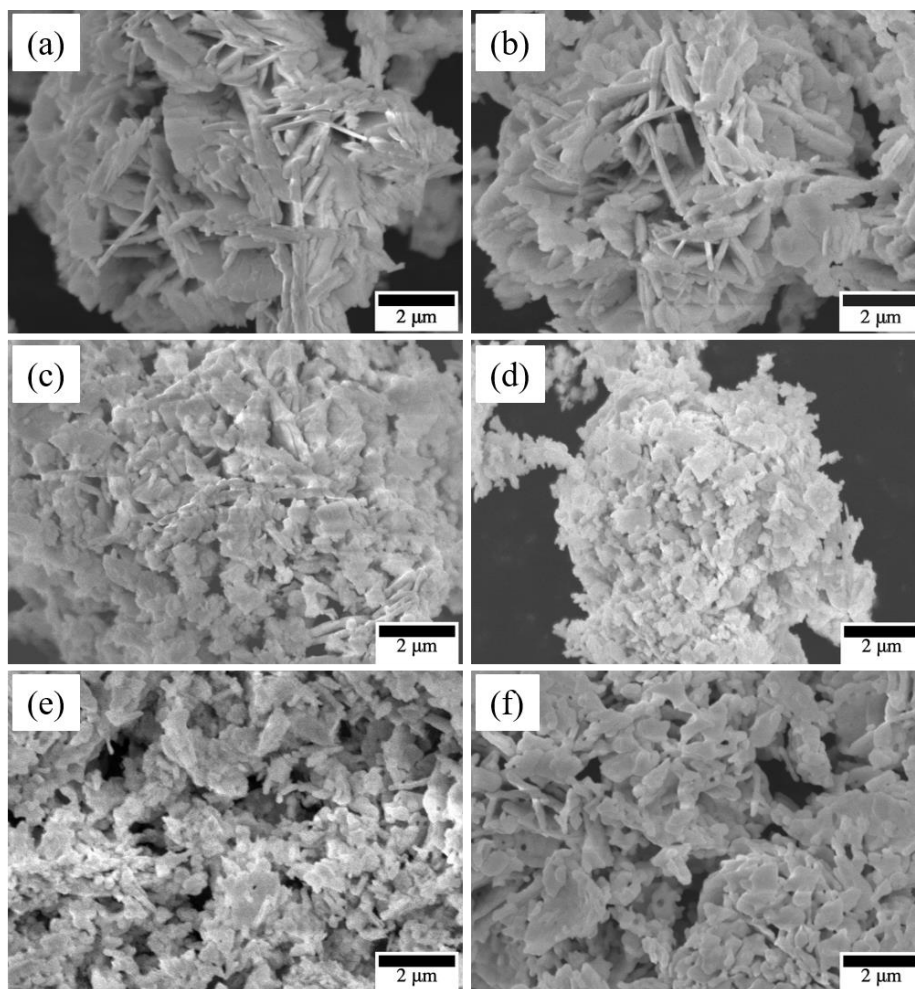
Figure 4 – Representative images of the samples $(BiO)_2CO_3$ (a), Bi-300°C (b), Bi-350°C (c), Bi-370°C (d), Bi-380°C (e), and Bi-400°C (f).

The optical properties of the bismuth precursor $((BiO)_2CO_3)$ and the samples synthesized at different temperatures were measured by UV-vis diffuse reflection spectroscopy and calculated by Tauc method[26], as seen in Figure 5 and Table 2. The absorbing edge of the precursor materials and the sample treated at 300°C are located in the same wavelength range between 354 and 375 nm, and this is also observed by bandgap energies with values of 3.4 and 3.3 eV, respectively, showing that there were no significant changes in the electronic structure of the pristine bismuth subcarbonate, and the sample calcined at 300°C. The same results were observed concerning the crystallographic structure of these samples, seen in XRD and Raman data, revealing the high stability of the carbonate, which decomposes around 350°C, as showed by XRD and TG/DTG results.[24] The sample annealed at 350°C showed a redshift of the absorption edge with two different bandgaps 3.2 and 2.3 eV, related to the presence $(BiO)_2CO_3$ and β-Bi_2O_3 phase, respectively, indicating the formation of two crystalline phase, as observed by XRD and Raman analysis.[27]

The precursor calcination at 370°C showed a change in the spectrum profile, disappearing the absorption edge in 3.3 eV related to $(BiO)_2CO_3$, indicating that all the carbonate was decomposed to form β-Bi_2O_3 and α-Bi_2O_3 phase, showing the bandgap value at 2.3 eV and 2.7 eV, respectively. This result is agreement with observed by Raman analysis and opposite to XRD result, it happened because is well-known that Raman and DRS is more sensitive for identification of a second phase than XRD, especially when the main XRD peaks are overlapped. Increasing the treatment temperature to 380°C, β-Bi_2O_3 was partially converted into α-Bi_2O_3, formatting a new heterostructure, β-Bi_2O_3/α-Bi_2O_3, with a bandgap value of 2.8 eV. However, above 400°C, the entire phase β-Bi_2O_3 present in the heterostructure is converted to phase α-Bi_2O_3, with the bandgap value 2.8 eV. Therefore, the samples treated above 350ºC are active by visible radiation, showing that the proposed method was able to promote the formation of the heterostructure with controlled physical-chemical properties.
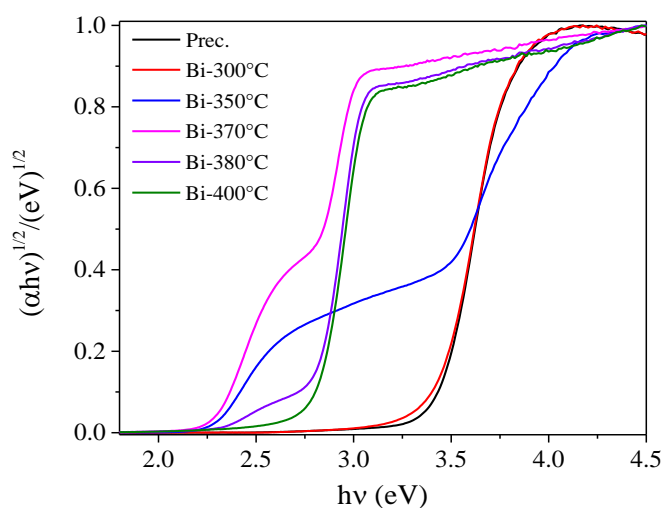
Figure 5 – Plots of $(\alpha h\upsilon)^{1/2}$ vs. photon energy ($h\upsilon$) obtained by the Tauc equation from DRS spectra for samples as-obtained.

Table 2 – The crystalline phase identified by diffractogram pattern and bandgap values obtained from the Tauc plot extrapolation.

Samples	Crystalline phase	Bandgap (eV)	
Prec.	$(BiO)_2CO_3$	3.4	-
Bi-300ºC	$(BiO)_2CO_3$	3.3	-
Bi-350ºC	**$(BiO)_2CO_3$ and β-Bi_2O_3**	**3.2**	**2.3**
Bi-370ºC	β-Bi_2O_3	2.7	2.3
Bi-380ºC	**β-Bi_2O_3 and α-Bi_2O_3**	**2.8**	**2.3**
Bi-400ºC	α-Bi_2O_3	2.8	-

1.5. Photoactivity of the semiconductors

The photocatalytic performances of the Bi-based materials were evaluated using the oxidation of methylene blue (MB) dye under UV and visible irradiation, as observed in Figure 6. The activity of the prepared samples was compared to the photolysis of the MB in the same experimental condition, demonstrating that this effect has little contribution to discoloration of the dye, ~1 and 11%, to the catalytic tests under UV and visible radiation, respectively. Under UV radiation, the primitive $(BiO)_2CO_3$ exhibited higher activity in MB photooxidation, followed by the sample treated at 300°C with an efficiency of 91 and 38%, respectively, after 60 min under UV irradiation (Figure 6a). However, the synthesized samples above 300°C showed lower photocatalytic activity. The formed heterostructures $(BiO)_2CO_3/\beta-Bi_2O_3$ and $\beta-Bi_2O_3/\alpha-Bi_2O_3$ exhibited efficiencies of approximately 16 and 31%, respectively.

Meanwhile, the prepared isolated phases ($\beta-Bi_2O_3$ and $\alpha-Bi_2O_3$) showed MB dye discoloration of 32 and 28%, respectively (Figure 6a). Therefore, under UV radiation, the untreated Bi-based sample showed better photocatalytic performance than the prepared samples. As shown by DRS spectra, all analyzed samples are optically active under UV radiation. Thus, the difference in the photocatalytic performance of the samples is attributed to the effects promoted by calcination, which at high temperatures coalesce the particles and sinter the pores of the materials, decreasing the number of active sites available for interaction with the reagent molecule, an essential factor for photocatalytic processes.[28]

Regarding the photocatalytic performance under visible radiation, the pristine $(BiO)_2CO_3$ (precursor) and the sample treated at 300°C showed poor catalytic activity, degrading the MB dye approximately 23 and 18%, respectively. Because, both samples are inactive under visible radiation, as demonstrated in the DRS data. The photocatalytic performance exhibited by both samples is due to the sensitization process resulting from the adsorption of methylene blue molecules on the surface of the analyzed oxides.[29,30] On the other hand, the photocatalytic test using the annealed samples above 300°C shown good results for methylene blue dye discoloration. The annealed samples at 350°C has the capacity to discoloration 40% of the methylene blue dye after 300 min under visible radiation, while samples prepared at 370°C, 380°C, and 400°C under the same experimental conditions induced discoloration of methylene blue of 56, 41, and 42% respectively. Therefore, the heterostructured samples exhibited a good photocatalytic performance under visible radiation, due to the increase in the radiation harvesting. Additionally, the sample obtained

at 370°C exhibited the best photocatalytic performance due to the heterostructure formation between β-Bi_2O_3/α-Bi_2O_3 that can promote a spatial separation of the electron/hole pair and consequently increase the electron/lifetime, as demonstrated before for our research group in similar heterostructure.[17,24]
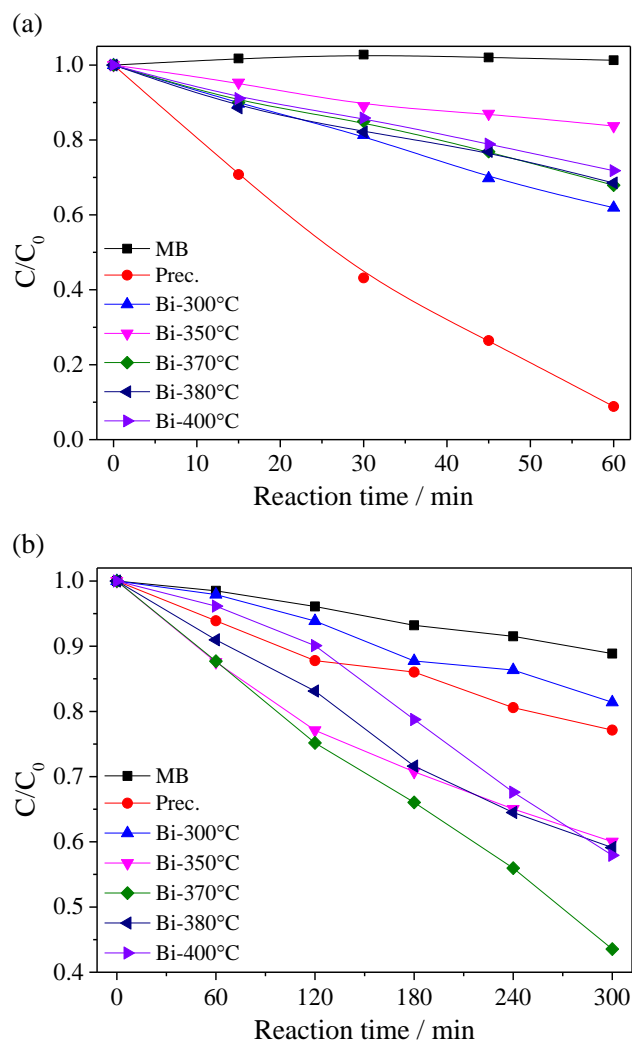
Figure 6 – Photocatalytic activity of as-prepared photocatalyst under UV (a) and visible irradiation (b).

The quantitative analysis of the photoactivity of the synthesized samples against the discoloration of MB dye was obtained according to the apparent first-order kinetic reactions shown in Table 3. According to the determined apparent rate constants, the photocatalytic activity under UV irradiation had the following trend: Precursor (($BiO)_2CO_3$) > 300°C > 370°C > 380°C > 400°C >350°C. It was found that increasing the calcination temperature affect negatively the photocatalytic activity of the synthesized samples under UV irradiation test. It is in agreement with expected, since under UV light all crystalline phase evaluated could be activated. However, due to the wide band gap of $Bi_2O_2CO_3$ sample, it exhibit a

valence band more negative than Bi_2O_3 phases. Additionally, the increase in calcination temperature can result in particle sizes higher and denser associated with of surface groups (active sites) loss and it can be deleterious for photocatalytic application

On the other hand, the experiments performed under visible irradiation had the following trend of the photoactivity: 370°C > 400°C > 380°C > 350°C > 300°C > Precursor ($(BiO)_2CO_3$). The best photocatalytic performance of synthesized samples above 300°C was expected, mainly due to their electronic structure and formation of heterojunctions, increasing the absorption of incident radiation and reducing the rate of recombination charges photoinduced, improving the lifetime, density, and mobility of the carrier, demonstrating that both isolated phases and prepared heterostructures are promising candidates for catalytic experiments under solar radiation.

Table 3 – Apparent constant of first-order rate (k_{app}) and the correlation coefficient (R^2) obtained in the discoloration of methylene blue driven by catalysts prepared under UV-Vis radiation.

Samples	UV Irradiation		Visible Irradiation	
	k_{app} x 10^{-4}	R^2	k_{app} x 10^{-4}	R^2
Precursor	38.9	0.9301	50.8	0.9832
Bi-300°C	8.1	0.9926	42.1	0.9719
Bi-350°C	3.0	0.9667	100.9	0.9831
Bi-370°C	6.2	0.9827	161.0	0.9819
Bi-380°C	6.0	0.9842	108.8	0.9929
Bi-400°C	5.4	0.9931	112.0	0.9413

4. Conclusion

In summary, we have demonstrated a facile calcination method to obtain Bi-based heterostructures with the potential to be applied in photocatalytic applications under UV and visible radiation. We showed that the materials composition and structure could be tuned by the calcination temperature. Additionally, the morphology and optical properties are modified and controlled by the calcination temperature. The $(BiO)_2CO_3$ sample exhibited the best photocatalytic performance on the MB degradation under UV radiation. On the other hand, under visible-radiation, the Bi-based heterostructures showed the best performance on the MB degradation, due to its lower band gap value and higher electron/hole lifetime.

5. Acknowledgment

6. Bibliography

[1]   W. Li, *Phys. Status Solidi RRL*, **9**, 10–27 (2015).

[2]   V.R. de Mendonça, O.F. Lopes, A.E. Nogueira, G.T.S.T. da Silva, and C. Ribeiro, Challenges of Synthesis and Environmental Applications of Metal-Free Nano-heterojunctions, in: Ed. by Inamuddin, G. Sharma, A. Kumar, E. Lichtfouse, and A.M. Asiri, Nanophotocatalysis and Environmental Applications, Springer International Publishing, Cham (2019), pp. 107–138.

[3]   C. Karthikeyan, P. Arunachalam, K. Ramachandran, A.M. Al-Mayouf, and S. Karuppuchamy, *Journal of Alloys and Compounds*, **828**, 154281 (2020).

[4]   S. Zhu and D. Wang, *Adv. Energy Mater.*, **7**, 1700841 (2017).

[5]   J. Tian, Q. Shao, J. Zhao, D. Pan, M. Dong, C. Jia, T. Ding, T. Wu, and Z. Guo, *Journal of Colloid and Interface Science*, **541**, 18–29 (2019).

[6]   J. Wojnarowicz, T. Chudoba, and W. Lojkowski, *Nanomaterials*, **10**, 1086 (2020).

[7]   A.E. Nogueira, L.S. Ribeiro, L.F. Gorup, G.T.S.T. Silva, F.F.B. Silva, C. Ribeiro, and E.R. Camargo, *International Journal of Photoenergy*, **2018**, 1–10 (2018).

[8]   G.T.S.T. da Silva, K.T.G. Carvalho, O.F. Lopes, E.S. Gomes, A.R. Malagutti, V.R. Mastelaro, C. Ribeiro, and H.A.J.L. Mourão, *ChemCatChem*, **9**, 3795–3804 (2017).

[9]   G. Iervolino, I. Zammit, V. Vaiano, and L. Rizzo, *Top Curr Chem (Z)*, **378**, 7 (2020).

[10]   J.A. Herron, J. Kim, A.A. Upadhye, G.W. Huber, and C.T. Maravelias, *Energy Environ. Sci.*, **8**, 126–157 (2015).

[11]   X. Ren, M. Gao, Y. Zhang, Z. Zhang, X. Cao, B. Wang, and X. Wang, *Applied Catalysis B: Environmental*, **274**, 119063 (2020).

[12]   M. Miodyńska, A. Mikolajczyk, B. Bajorowicz, J. Zwara, T. Klimczuk, W. Lisowski, G. Trykowski, H.P. Pinto, and A. Zaleska-Medynska, *Applied Catalysis B:*

Environmental, **272**, 118962 (2020).

[13]   L. Zhou, W. Wang, H. Xu, S. Sun, and M. Shang, *Chem. Eur. J.*, **15**, 1776–1782 (2009).

[14]   O.F. Lopes, K.T.G. Carvalho, G.K. Macedo, V.R. de Mendonça, W. Avansi, and C. Ribeiro, *New J. Chem.*, **39**, 6231–6237 (2015).

[15]   G. Cai, L. Xu, B. Wei, J. Che, H. Gao, and W. Sun, *Materials Letters*, **120**, 1–4 (2014).

[16]   C. Li, Y. Ma, S. Zheng, C. Hu, F. Qin, L. Wei, C. Zhang, S. Duo, and Q. Hu, *Journal of Colloid and Interface Science*, **576**, 291–301 (2020).

[17]   O.F. Lopes, K.T.G. Carvalho, W. Avansi, and C. Ribeiro, *J. Phys. Chem. C*, **121**, 13747–13756 (2017).

[18]   J. Zhang, J.H. Bang, C. Tang, and P.V. Kamat, *ACS Nano*, **4**, 387–395 (2010).

[19]   S. Jabeen, J. Iqbal, A. Arshad, J. Williams, S. Samarin, and M. Rani, *Journal of Alloys and Compounds*, **842**, 155840 (2020).

[20]   G.T.S.T. da Silva, K.T.G. Carvalho, O.F. Lopes, and C. Ribeiro, *Applied Catalysis B: Environmental*, **216**, 70–79 (2017).

[21]   K.T.G. Carvalho, A.E. Nogueira, O.F. Lopes, G. Byzynski, and C. Ribeiro, *Ceramics International*, **43**, 3521–3530 (2017).

[22]   M.A. Ferreira, G.T.S.T. da Silva, O.F. Lopes, V.R. Mastelaro, C. Ribeiro, M.J.M. Pires, A.R. Malagutti, W. Avansi, and H.A.J.L. Mourão, *Materials Science in Semiconductor Processing*, **108**, 104887 (2020).

[23]   R. Bueno, O. Lopes, K. Carvalho, C. Ribeiro, and H. Mourão, *QN*, (2019).

[24]   O.F. Lopes, K.T.G. Carvalho, W. Avansi, D.M.B. Milori, and C. Ribeiro, *RSC Adv.*, **8**, 10889–10897 (2018).

[25]   H.-Y. Jiang, P. Li, G. liu, J. Ye, and J. Lin, *J. Mater. Chem. A*, **3**, 5119–5125 (2015).

[26]   P. Makuła, M. Pacia, and W. Macyk, *J. Phys. Chem. Lett.*, **9**, 6814–6817 (2018).

[27]   Md.T. Uddin, Y. Nicolas, C. Olivier, W. Jaegermann, N. Rockstroh, H. Junge, and T. Toupance, *Phys. Chem. Chem. Phys.*, **19**, 19279–19288 (2017).

[28]   T. Zhao, J. Zai, M. Xu, Q. Zou, Y. Su, K. Wang, and X. Qian, *CrystEngComm*, **13**, 4010 (2011).

[29]   J. Diaz-Angulo, I. Gomez-Bonilla, C. Jimenez-Tohapanta, M. Mueses, M. Pinzon, and F. Machuca-Martinez, *Photochem. Photobiol. Sci.*, **18**, 897–904 (2019).

[30]   L. Pan, J.-J. Zou, X. Zhang, and L. Wang, *J. Am. Chem. Soc.*, **133**, 10000–10002 (2011).